Cross-conjugated BODIPY pigment for highly efficient dye sensitized solar cells

Md Faiz Shah, Antoine Mirloup, Towhid Chowdhury, Ryuji Kaneko, Alexandra Sutter, Abdulkader Hanbazazah, Anas Ahmed, Jae-Joon Lee, M. Abdel-Shakour, Nicolas Leclerc, et al.

Cross-Conjugated BODIPY Pigment for Highly Efficient Dye Sensitized Solar Cells

Md Faiz Shah,[a‡] Antoine Mirloup,[b ‡] Towhid H. Chowdhury,[c.d] Ryuji Kaneko,[c] Alexandra Sutter,[b] Abdulkader S. Hanbazazah,[a] Anas Ahmed,[a] Jae-Joon Lee,[d] M. Abdel-Shakour,[c] Nicolas Leclerc,[b*] Ashraful Islam.[c *]

[a] Department of Industrial Engineering, University of Jeddah, Kingdom of Saudi Arabia

[b] Institut de Chimie et Procédés pour l'Energie, l'Environnement et la Santé (ICPEES), Université de Strasbourg, CNRS, UMR 7515, 25 rue Becquerel, 67087 Strasbourg, Cedex 02, France

[c] Photovoltaic Materials Group, Center for Green Research on Energy and Environment Materials, National Institute for Materials Science, Sengen 1-2-1, Tsukuba, Ibaraki 305-0047, Japan.

[d] Department of Energy & Materials Engineering & Research Center for Photoenergy Harvesting and Conversion Technology (*phct*), Dongguk University, Seoul 04620, Republic of Korea.

[‡] Md Faiz Shah and Antoine Mirloup contributed equally.

Corresponding author: Islam.Ashraful@nims.go.jp; leclercn@unistra.fr

Keywords: Dye sensitized solar cells; Cross conjugation; BODIPY Dyes; Panchromatic sensitizer; Co-sensitization; NIR absorption

Abstract

In this study, we report a new BODIPY-based design, called *cross-conjugated design*, that takes advantage of the α- and β-positions functionalization of the BODIPY core. After synthesis, and compared to a more standard BODIPY dye, using similar functional groups and based on a horizontal design, called ***h*-BOD**, the new cross-conjugated BODIPY dye (***cc*-BOD)** exhibits clearly the highest conjugation and light harvesting properties. Consequently, when used as photosensitizers in dye-sensitized solar cells (DSSCs), an impressive improvement of power conversion efficiency (PCE) has been observed, with a PCE of 6.02% with broad incident photon

to current conversion efficiency (IPCE) for ***cc*-BOD,** compared to only 3.7% for ***h*-BOD**. Moreover, by co-sensitizing a DSSC with the two complementary absorbing dyes ***h*-BOD** and ***cc*-BOD**, we further improved the PCE up to 6.2 %.

1. Introduction

Since its first inception in 1992 by Gratzel [1], dye sensitized solar cells (DSSCs) have been a popular choice of solar energy source due to their versatile impacts, such as easy fabrication process, light weight and flexible physical structure. Generally, DSSCs are fabricated with an electrode, a dye sensitizer, electrolytes, a counter electrode sandwiched between two transparent conducting substrates [2, 3]. Among all the other components, the dye contributes to determine the photovoltaic response of the overall device by harvesting efficiently and by injecting the photo-generated electrons and holes into, respectively, the semiconductor oxide and the redox electrolyte, with matched energy levels [4, 5]. In this regard, a vast amount of dyes have been implemented in DSSCs, which can be categorized into metal-based dyes and organic dyes. In terms of photovoltaic responses, metal-based dyes show superior performances but due to low yield and scarcity of source materials they remain quite unattractive [6, 7]. Metal free organic dyes with easy synthesis processes have shown promising or even equal photovoltaic performances in DSSCs [8-11]. The advantages of organic dyes over metal-based dyes rely on their ability to absorb light in specific wavelengths with high molar extinction coefficient [12-14]. The molecular engineering and tailoring of different light absorbing functional groups can lead to a light harvesting tuning over a broad spectral range resulting in highly efficient DSSCs [15-21]. Boron-dipyrromethene (BODIPY) dyes are among the most widely considered chromophores thanks to their unique optical properties, including high absorption coefficients in the visible and NIR ranges and high fluorescence quantum yields [22]. In addition, BODIPY dyes often exhibit a high stability in various media. Last but not least, the high number of reactive chemical positions allow a very fine tuning of their opto-electronical properties. Therefore, BODIPY-based molecules have found application in a numerous field of application such as Organic Light Emitting Diodes (OLED) [23] (bio)-labeling [24] photodynamic therapy [25], or photovoltaic devices, including organic [26] and hybrid technologies [27].

The numerous chemical modifications of the BODIPY core, have made it possible to highlight

the weak points of this chemical building block that need to be improved to increase the dye performances in DSSC devices and consequently the power conversion efficiencies (PCE) [28-31]. These issues are the following: i) A weak regeneration driving force between the ground state oxidation potential (highest occupied molecular orbital, HOMO) of the dye and the redox potential of the iodine/iodide redox electrolyte [32]. ii) A weak driving force for the injection of the excited state electron into the TiO_2 resulting from the usual inappropriate alignment of the BODIPY dyes lowest unoccupied molecular orbital (LUMO) energy level is too near to the conduction band (CB) of TiO_2 photoanode. Consequently, the BODIPY based DSSCs often show low incident photon-to-current conversion efficiency (IPCE) [33, 34]. iii) A strong aggregation of the flat BODIPY sensitizers on the surface of TiO_2 leading to low charge recombination, which decreases the device open-circuit photovoltage.

Chemical engineering has already brought some positive answers to these issues, such as the variation of the number of functionalized groups grafted onto the 3,5-positions of the BODIPY core, allowing to tune the final dye LUMO level [35]. Similarly, the aggregation related issue could be addressed by playing with the steric hindrance of side chains. For instance, the boron substitution by inert alkynyl-oligoethylene glycol chains has shown to be a good strategy to increase both solubility and stability and to suppress the dye aggregation.[36, 37] However, despite the positive evolution of chemical designs and device efficiencies, the rationalization of the chemical structure – photovoltaic properties relationship is still difficult. Therefore, new dye investigations are required. In a recent review related to the use of BODIPY dyes for the DSSC application, Klfout et al.[28] defined two distinct dye design strategies (see Figure 1) i.e. the *vertical design* in which the functional electron-donor (D) and electron-acceptor (A) groups are grafted vertically to the BODIPY core main plane, by using the 3- and 5-positions (usually for D) on one side and the 8 (meso)-position for the A group grafting ; and the *horizontal design* in which the D and A groups are grafted horizontally, on each side of the BODIPY core, by using the 2- and 6-positions of the BODIPY molecule.

In this study, we report an innovative design, called *cross-conjugated design*, by combining the horizontal and vertical design in one single dye (see Figure 1). Indeed, we used three different (2, 3 and 5) positions to substitute the electron donor groups and the position 6 to graft the electron-acceptor/anchoring group (see Figure 1, ***cc*-BOD**). In order to validate this chemical design, we

also synthesized a reference model, based on the only horizontal design by removing the donor groups in the 3- and 5-positions (see Figure 1, ***h*-BOD**). The synthesis, spectroscopic characterization, electrochemistry, and photovoltaic properties of these compounds have been evaluated in detail. The cross-conjugated BODIPY dye, ***cc*-BOD**, exhibits a very broad absorption spectrum up to 760 nm, when adsorbed on TiO_2 photoanode and leads to a high PCE value of 6.02% when used as sensitizer in a DSSC. Interestingly, the simpler ***h*-BOD** dye showed a narrower and blue-shifted absorption range, limited to 650 nm leading to a lower PCE value of only 3.7%. The differences in the photovoltaic responses validate our new cross-conjugated design. Finally, by utilizing the complementary absorption spectra of both dyes, co-sensitized DSSCs were successfully fabricated to a slightly increased PCE of 6.20%.

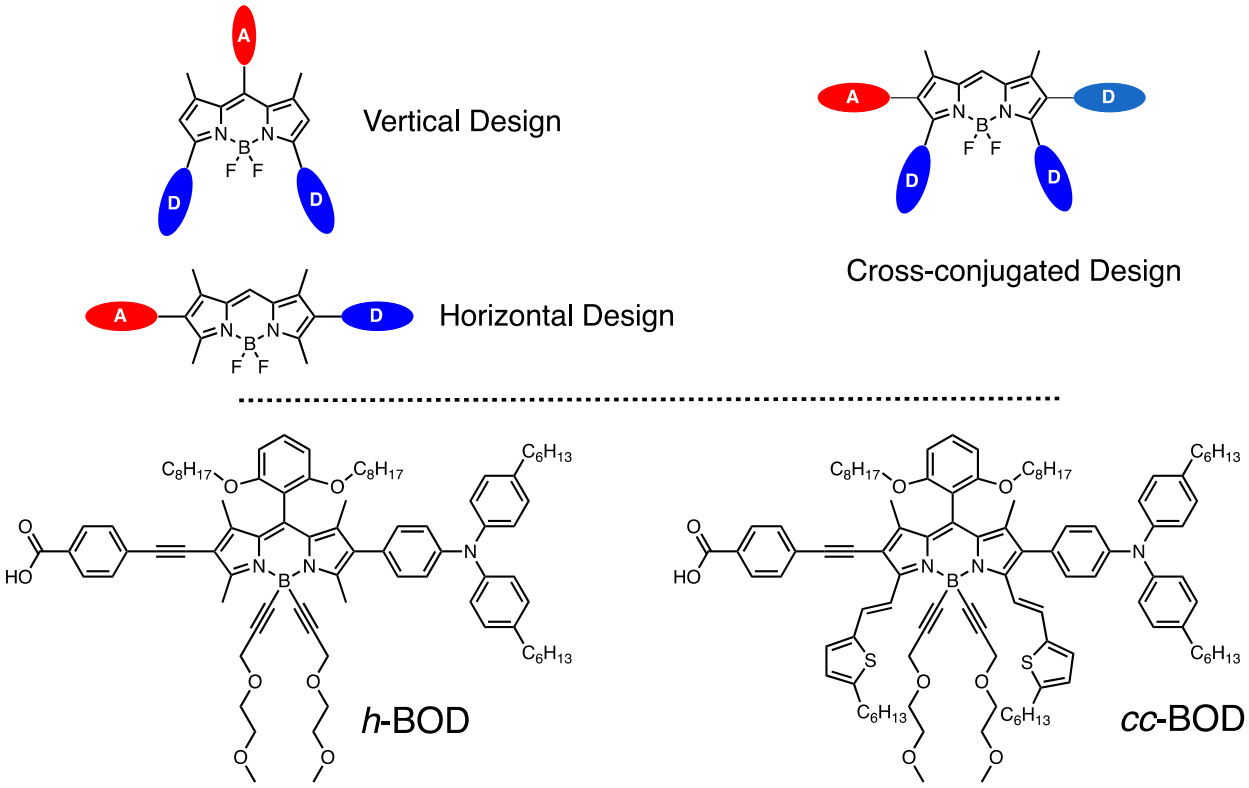

Figure 1. *Top*. Chemical design strategies; *Bottom*. Molecular structures of *h*-BOD and *cc*-BOD

2. Experimental Section

The starting compounds in Scheme 1 were prepared according to the reported works [32-34] and given in details at the supporting information S3 and Figure S1-S5. The TiO_2 on top of the Fluorine-doped tin oxide (FTO) coated glass and the DSSCs were fabricated following the

methodology of our previous work [36]. Briefly, prior to dye adsorption the TiO_2 film was further treated with 0.1M solution of HCl. A solution of BODIPY dyes (2×10^{-4} M) and deoxycholic acid (1×10^{-2} M) in acetonitrile/tert-butyl alcohol (1/1, v/v) was used as a dye bath for a single *h*-BOD or *cc*-BOD based DSSCs. For the co-sensitized DSSCs, the TiO_2 photoanodes were immersed into a mix dye solution of *h*-BOD and *cc*-BOD with molar ratio of 1:2 (1.3×10^{-4} M: 2.6×10^{-4} M) containing 1×10^{-2} M deoxycholic acid in 1:1 acetonitrile and *tert*-butyl alcohol. The electrodes were immersed in the dye solutions and then kept at 35 °C for 12 h to adsorb the dye onto the TiO_2 surface. Each BODIPY-coated TiO_2 film and a Pt-coated conducting glass were separated by a 40 μm thick polymer-based spacer (Surlyn) and sealed by heating the Surlyn frame at 100 °C. An electrolyte consisting of a mixture of I_2 (0.05 M), LiI, (0.1 M), dimethylpropyl-imidazolium iodide (0.6 M), and *tert*-butylpyridine (0.05 M) in acetonitrile was used. **BODIPY** dye coated TiO_2 films were immersed in 0.1 M TBAOH solution (1:1 mixture of H_2O and ethanol) to desorb the dyes. The absorption peak of each resulting **BODIPY** single and co-sensitized dye solution was used to estimate the amount of adsorbed dye. The details method for the characterization of solar cells has been provided in supporting information S1-S2.

3. Results and discussion

3.1. Synthesis of BODIPY dyes *h*-BOD and *cc*-BOD

The cross-conjugated design involved in this work, is partially inspired by the work of Grätzel et al. on the YD2-*o*-C8 porphyrin derivative [38]. Indeed, based on our knowledge regarding the functionalization of BODIPY molecules for light harvesting applications, we have grafted vinyl-thiophen groups on the 3- and 5-positions [39], in order to obtain a wide electronic delocalization. The original idea of this work is to take advantage of BODIPY's chemical versatility to add a lateral push-pull effect by functionalizing in 2- and 6- positions. The synthesis of compounds **1**, **A** and **B** could be found in the supplementary information as well as details regarding the chemical analysis of all compounds. The 3,5-difunctionalized BODIPY 2 has been obtained by a Knoevenagel reaction between the BODIPY 1, never reported in literature, and the aldehyde **A** (usually in excess) in the presence of piperidine and trace amounts of *p*-TsOH. The color of the reaction mixture was used to follow the reaction steps (magenta for mono-substitution and blue for the expected di-substitution). From this stage, the two ***h*-BOD** and ***cc*-BOD** dyes are synthesized in the same way, following exactly the identical synthesis steps. Thus, the second

step made use of a Grignard reagent capable of transforming the BF_2 fragment into $B(alkynylPEG)_2$ (Scheme 1). The substitution of the first iodo group with the triphenylamine derivative, **B**, was achieved through Suzuki coupling in presence of K_2CO_3 and $[Pd(PPh_3)_2Cl_2]$ (compounds **5** and **6**). While, the second Iodo group was substituted with phenylcarboxyester using NEt_3 and copper iodide in presence of $[Pd(PPh_3)_2Cl_2]$ catalyst to give compounds **7** and **8**, respectively. Finally, the resulting esters were hydrolyzed to the acids, leading to the target dyes ***h*-BOD** and ***cc*-BOD**, respectively. All the synthesized compounds were characterized using NMR (see supplementary information).

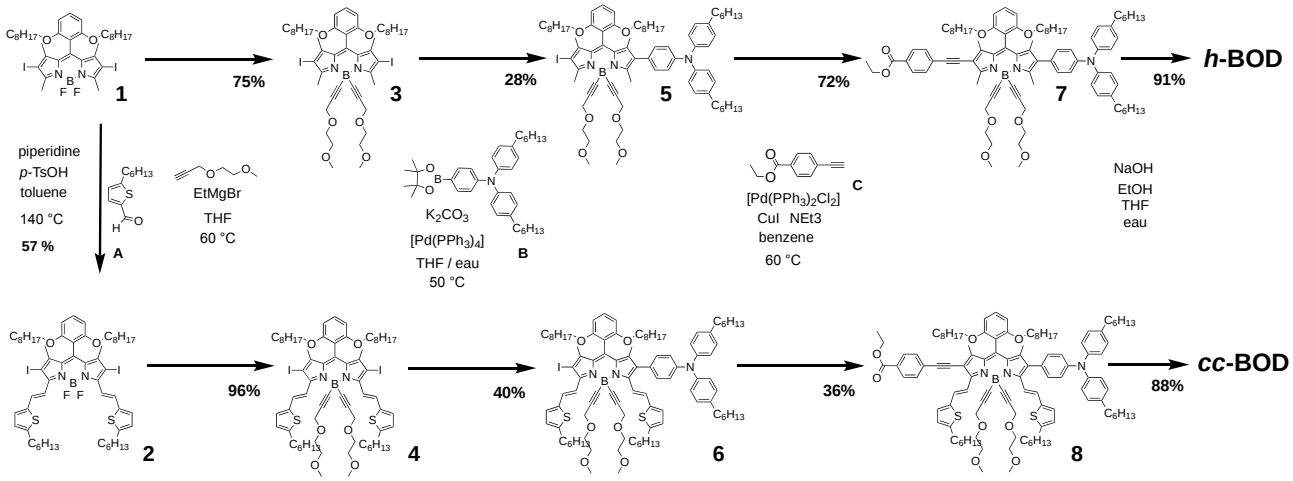

Scheme 1. Synthetic routes for the Bodipy dyes, ***h*-BOD** and ***cc*-BOD**.

3.2. Optical and electrochemical properties

The optical characteristics, of both new BODIPY dyes were inspected and are summarized in Table 1. Absorption and emission spectra in THF solution of both dyes are illustrated in Figure 2. The model compound, ***h*-BOD**, exhibits a quite narrow two bands absorption spectrum. The lower energy band, centered on 553 nm, has strangely no vibronic signature, as usually observed in BODIPY-based dyes. The related molar extinction coefficient value is of 54000 $M^{-1}.cm^{-1}$. The band at higher energy could be attributed to the triphenylamine group absorption. The ***h*-BOD** emission spectrum (See figure S6) shows a broad feature and a large stokes shift of 2600 cm^{-1} as regards to the absorption. This is a signature of a strong molecular polarization in the excited state, as already shown in literature for many ß-functionalized BODIPY dye [40]. The ***cc*-BOD** spectroscopic features are quite different. Its absorption spectrum has three absorption maxima

and is significantly red-shifted compared to the model compound. The one with the lowest energy is at 688 nm and can be attributed to the $S_0 \rightarrow S_1$ transition [41]. This time, a clear vibronic structure can be observed, with a first shoulder at 628 nm and a second one, lower in intensity, at about 580 nm. The molar extinction coefficient associated with this transition is of 103000 $M^{-1}.cm^{-1}$. The second transition is around 400 nm and seems to be split. As described previously in the literature [39], this transition can be attributed to the absorption of vinyl-thiophene arms. However, because of the unsymmetrical functionalization of ***cc*-BOD** in the 2,6-positions, these two moieties are no longer equivalent in this case and consequently, the absorption is split into two bands. The last transition at 310 nm corresponds to the absorption of the triphenylamine group. The absorption properties characterization highlights very well the strong and positive impact of our new cross-conjugated design strategy with a dye that exhibits a broader and intense absorption all along the UV-visible range. The ***cc*-BOD** molecule emits light with a maximum located at 708 nm and a good quantum fluorescence efficiency of 33% (See figure S7). With the shoulder at lower energy, this band is characteristic of the BODIPY $S_1 \rightarrow S_0$ transition. This spectrum is the mirror image of the absorption spectrum and Stokes shift of around 410 cm^{-1} could be measured. From UV-visible solution measurements optical bandgaps have been measured, 2.06 eV and 1.71 eV, for ***h*-BOD** and ***cc*-BOD**, respectively.

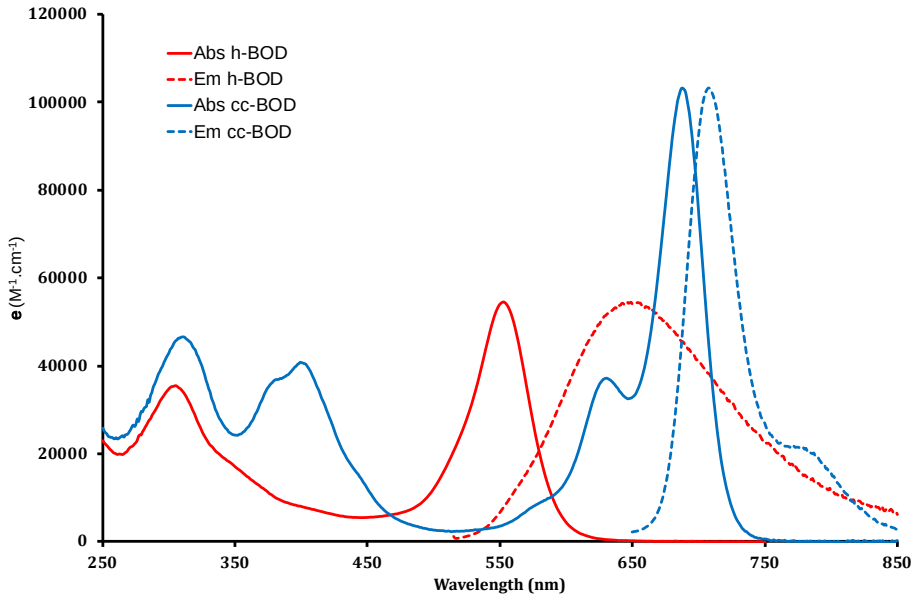

Figure 2. Absorption (solid trace) and emission (dashed line) spectra in THF of ***h*-BOD** and ***cc*-BOD**

Figure 3 shows the absorption spectra of ***h*-BOD** and ***cc*-BOD** dyes adsorbed on TiO_2 film. Due to carboxylic groups of dyes that interact with TiO_2, the spectra look broad. However, we clearly observed similar trends with the previous solution measurement, including a really much broader spectrum for the ***cc*-BOD** up to the NIR region as compared to the ***h*-BOD** dye.

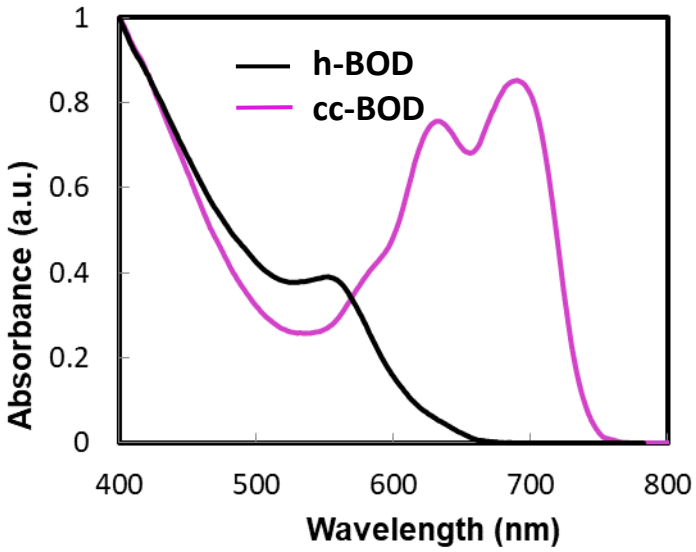

Figure 3. Absorption spectra of ***h*-BOD** and ***cc*-BOD** on TiO_2

To compute the electron transfer from the excited state of dye molecules to the conduction band of the respective TiO_2, the ionization potential (IP), equivalent to ground state oxidation potential, of ***h*-BOD** and ***cc*-BOD** anchored to TiO_2 film were also measured (Figure S8 and Figure S9) using a photoemission yield spectrometer (Riken Keiki AC-3E). The findings are summarized in Table 1. An expression $E_{0\ (D+/D^*)}$ = IP - $E_{0\text{-}0}$, has been utilized to evaluate the excited state oxidation potentials ($E_{0\ (D+/D^*)}$) levels of ***h*-BOD** and ***cc*-BOD** which showed values of -3.81 and -4.03 eV, respectively (Table 1). Compared with ***h*-BOD** cross-conjugated BODIPY dye, ***cc*-BOD** exhibits a decrease in the $E_{0\text{-}0}$ energy gap which leads to a red shift of the absorption bands with comparatively positive $E_{0\ (D+/D^*)}$ levels. The $E_{0\ (D+/D^*)}$ for ***h*-BOD** and ***cc*-BOD** are located over the conduction band edge of the TiO_2 [42]. Therefore, an efficient excited-state injection into the conduction band of TiO_2 is expected for the DSSCs fabricate with ***h*-BOD** and ***cc*-BOD dyes** (Figure 4). Apparently, the ground state oxidation potentials (equivalent to the ionization potential, IP) were more positive than the redox potential of I^-/I_3^- couple (-5.2 eV),

which indicates efficient dye regeneration. HOMO levels of ***h*-BOD** and ***cc*-BOD** were estimated, by cyclic voltammetry (CV), of about -5.49 eV and -5.36 eV, respectively (Figure S12 and Table S1). If considering the expected down-shifting of HOMO levels when the dyes are grafted onto the TiO_2, these HOMO level values, obtained by CV, are comparable with those obtained from PESA measurement on TiO_2 thin-films (deprotonation of the dye's carboxylic acid group to be covalently bonded to the TiO_2). The redox processes of the dyes were reproducible as shown in Figure S12b,c.

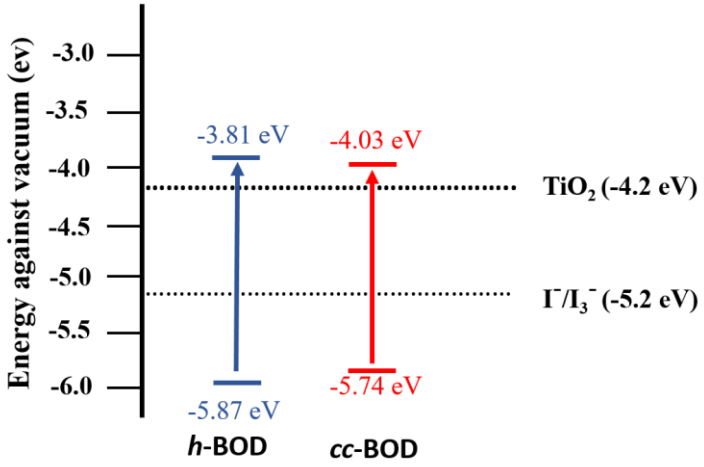

Figure 4. Energy-level diagram of ***h*-BOD** and ***cc*-BOD**, electrolyte and TiO_2.

Table 1. Photophysical parameters of ***h*-BOD** and ***cc*-BOD** Bodipy dyes.

Dyes	**λ_{abs} (nm)**	**ε (M^{-1} cm^{-1})**	**λ_{abs} on TiO_2 (nm)**	**λ_{em} (nm)**	***$E_{0\text{-}0}$*** **(eV)[a)]**	***IP*** **(eV)[b)]**	**E_0 D^+/D^* (eV)[c)]**
***h*-BOD**	553	54500	560	652	2.06	-5.87	-3.81
***cc*-BOD**	688	102000	696	708	1.71	-5.74	-4.03

[a)] Optical bandgap, $E_{0\text{-}0}$, was determined from UV-visible solution measurements.
[b)] Ionization potential, *IP*, of dyes adsorbed on nanocrystalline TiO_2 film measured using a photoemission yield spectrometer (Riken Keiki AC-3E) (see figure S8 and S9)
[c)] Excited-state oxidation potential, $E_{0\ (D+/D*)}$ was calculated from $E_{0(D^+/D^*)} = IP - E_{0-0}$.

3.3. Photovoltaic properties

Due to the high and appealing optoelectronic properties of ***cc*-BOD** and to a lesser extent of ***h*-BOD**, DSSCs were fabricated. The elaboration procedures have been reported in section 2. The photovoltaic parameters measured under AM 1.5G irradiation (100 mW cm^{-2}) have been summarized in Table 2 and shown in Figure 5. DSSCs sensitized with ***cc*-BOD** showed high photovoltaic response in the VIS-NIR region with a broad IPCE of approximately 60% in the 350-720 nm range (Figure 5a). Consequently, the ***cc*-BOD** dye-based devices exhibit pretty high photovoltaic performances with a PCE of 6.02% at maximum, including high photovoltaic parameters, short-circuit photocurrent density (J_{sc}) of 15.43 $mA.cm^{-2}$ and fill factors (*FF*) of 71%, except the open-circuit photovoltage (V_{oc}) which remains moderate (Figure 5b). Devices elaborated from ***h*-BOD** also showed IPCE > 60% but however on really blue-shifted and narrowest wavelength range (350-570 nm). Consequently, the PCE is much lower, 3.70%, mainly because of a decreased J_{SC} of 9.69 mA cm^{-2}. The *V*oc and *FF* being really close the ones previously measured with ***cc*-BOD**. From these photovoltaic measurements, it is rather obvious that the benefit of our new cross-conjugated design in terms of optical properties is responsible for the improved photovoltaic performances.

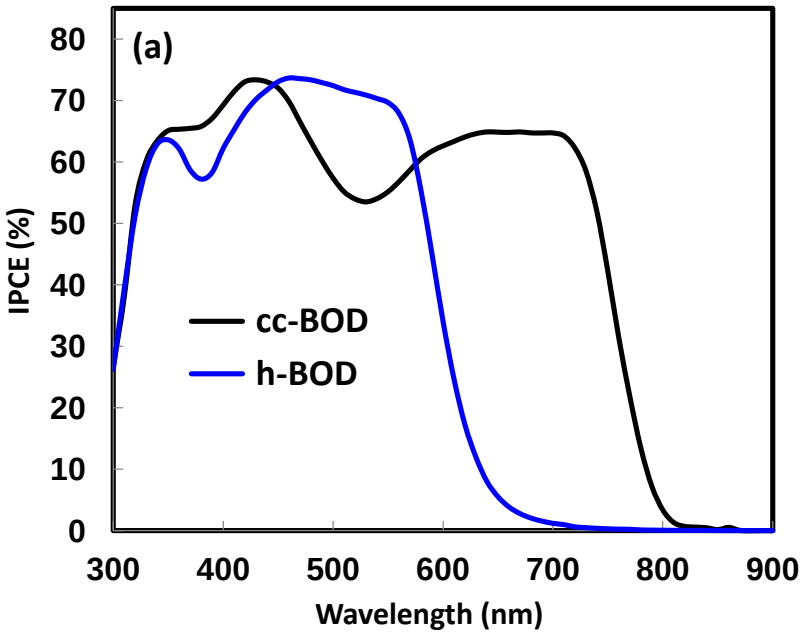

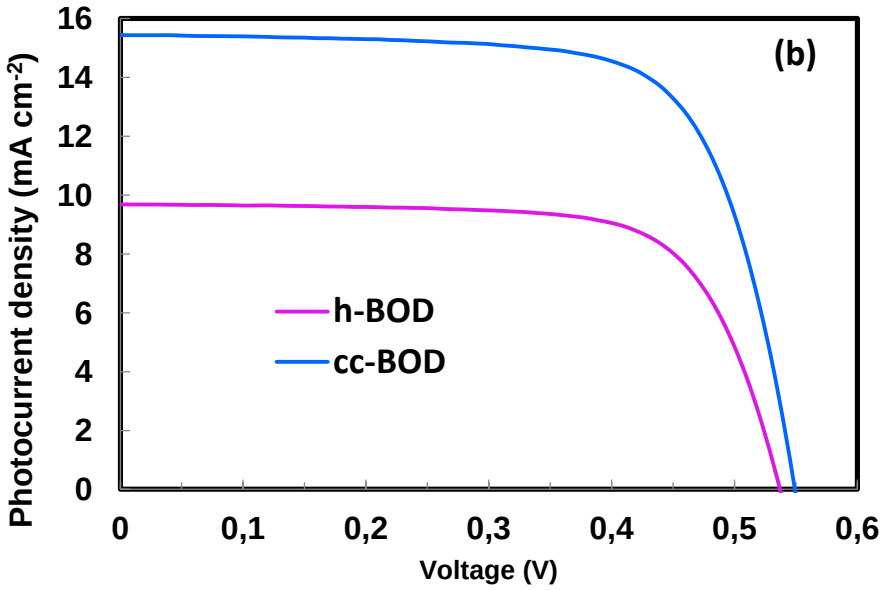

Figure 5. (a) IPCE spectra and (b) *J*-*V* curves for DSSCs with the ***h*-BOD** and ***cc*-BOD** Bodipy dyes. Electrolyte composed of 0.6 M dimethylpropyl-imidazolium iodide, 0.05 M I_2, 0.1 M LiI and 0.05 M 4-*tert*-butylpyridine in acetonitrile.

Table 2. Photovoltaic parameters of the fabricated DSSCs

Dye	J_{SC} [mA cm^{-2}]	V_{OC} [V]	*FF*	η [%]	IPCE [%]		Adsorbed amount of dye [mol cm^{-2}]
					530 nm	700 nm	
***h*-BOD**	9.69	0.537	0.711	3.70	71	1	1.23 x 10^{-7}
***cc*-BOD**	15.43	0.549	0.711	6.02	53	65	1.18 x 10^{-7}
***h*-BOD + *cc*-BOD (dye ratio; 1:2)**	16.07	0.561	0.688	6.20	69	63	8.03 x 10^{-8} (*h*-BOD) 7.83 x 10^{-8} (*cc*-BOD)

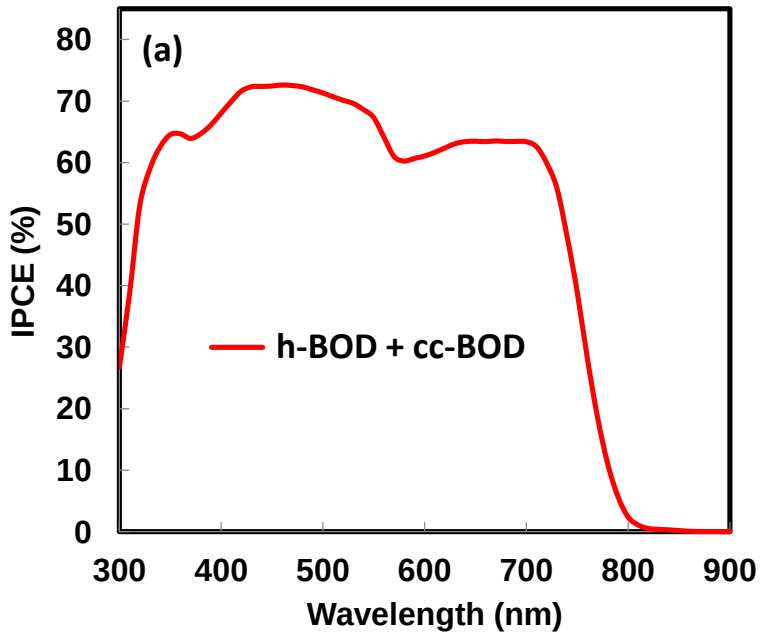

277

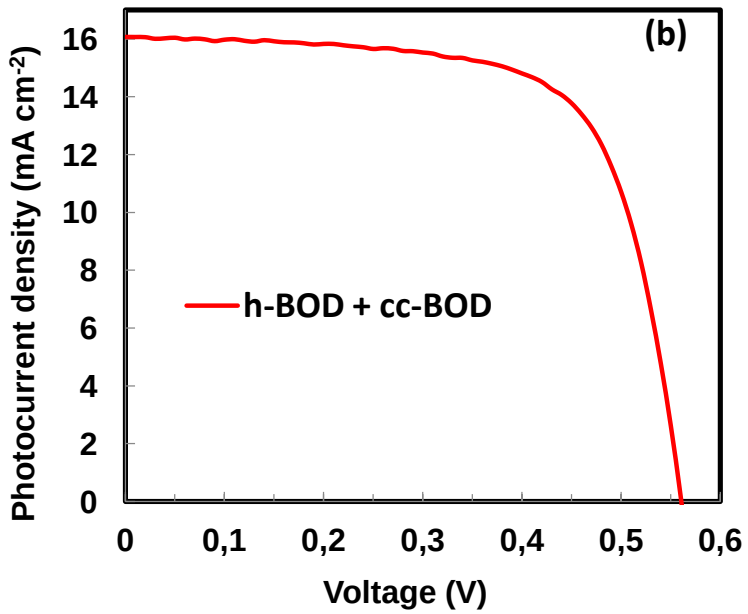

278

279

280 **Figure 6.** (a) IPCE spectra and (b) *J-V* curves for DSSCs co-sensitized with ***h*-BOD + *cc*-BOD**.
281 Electrolyte composed of 0.6 M dimethylpropyl-imidazolium iodide, 0.05 M I_2, 0.1 M LiI and
282 0.05 M 4-tert-butylpyridine in acetonitrile.

283

284 Interestingly, from Figure 3, one can noticed that despite a partial overlap of the absorption
285 spectra of both dyes, ***h*-BOD** exhibits a higher absorption feature in the 450-570 nm wavelength

range. It is therefore attractive to try to incorporate both dyes into the same device, thus called co-sensitized DSSC. As anticipated, the co-sensitized DSSC based on ***h*-BOD + *cc*-BOD** showed a high IPCE of more than 60% over the whole 330-720 nm region with an absorption onset up to 800 nm (Figure 6a). In comparison to the single ***cc*-BOD** dye, the co-sensitized ***h*-BOD + *cc*-BOD** system shows substantially increased IPCE in the visible region without decreasing IPCE in the NIR region. The IPCE at 530 nm increased from 53% for single ***cc*-BOD** dye to 69% for ***h*-BOD + *cc*-BOD.** Even though the adsorbed amount of ***cc*-BOD** in the ***cc*-BOD** alone cell decrease from 1.18×10^{-7} mol cm^{-2} to 7.83×10^{-8} mol cm^{-2} in the ***h*-BOD + *cc*-BOD** cell (Table 2), the IPCE spectrum of ***cc*-BOD** at 700 nm decreases only from 65% to 63% for co-sensitized ***h*-BOD + *cc*-BOD**, where mainly ***cc*-BOD** shows a photo-response. These results suggest that ***h*-BOD** does not affect the light harvesting efficiency of ***cc*-BOD** on TiO_2 film in the co-sensitized ***h*-BOD + *cc*-BOD** system. Consequently, an even improved photovoltaic performance in regard to previous elaborated DSSCs, inducing an enhanced J_{SC} of 16.07 mA cm^{-2}, was measured for the co-sensitized DSSC. The V_{OC} and FF remain quite unmodified (see Table 2, Figure 6b) and resulted in a PCE of 6.20%.

3.4. CEM and IMVS measurements

For determining the dynamics of charge recombination, the electron lifetime (τ) in the DSSCs is a key parameter to determine the which is related to the device V_{oc}. As the V_{oc} of a DSSC depends on the charge recombination reactions rather than molecular structures of the dyes, it is important to explore the role of the fabricated sensitizer based DSSCs in this aspect.[36] The relative conduction band positions and electron lifetimes in the DSSCs fabricated with either ***h*-BOD**, ***cc*-BOD** single dyes and ***h*-BOD + *cc*-BOD** co-sensitized dyes were examined to comprehend the difference of the measured V_{oc} for the DSSCs. Initially, the relative conduction band position of TiO_2 was measured by charge extraction method (CEM). Figure 7a shows that DSSCs sensitized with ***h*-BOD**, ***cc*-BOD** single dyes and ***h*-BOD + *cc*-BOD** co-sensitized dye display a similar linear increase in electron density as a function of V_{oc}. This indicates that ***h*-BOD**, ***cc*-BOD** single dyes and ***h*-BOD + *cc*-BOD** co-sensitized dye cells have the same conduction band edge of TiO_2 irrespective to the molecular structures and co-sensitization. We have further investigated the electron lifetime (τ, which reflects the degree of electron recombination) of the DSSCs sensitized with ***h*-BOD**, ***cc*-BOD** single dyes and ***h*-BOD + *cc*-**

BOD dyes by means of intensity-modulated photovoltage spectroscopy to understand the differences between the V_{oc} values of the respective DSSCs which is shown in Figure 7 (b). It is clear that at a fixed $V_{OC,}$ the lifetime decreases as ***h*-BOD + *cc*-BOD** > ***cc*-BOD** > ***h*-BOD**, which is in accord with the order of decreasing V_{OC} observed in the respective DSSCs. The longer lifetime observed for the ***h*-BOD + *cc*-BOD** based DSSC compared to cc-**BOD** and ***h*-BOD** based DSSCs suggests that the co-sensitized DSSC significantly suppressed the recombination of electrons in the TiO_2 film with I_3^-.

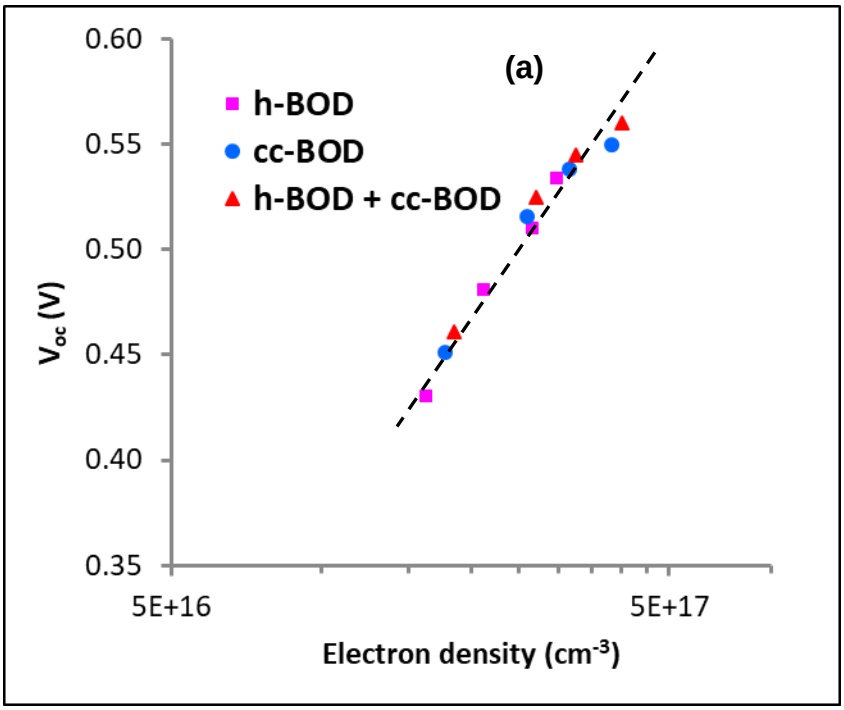

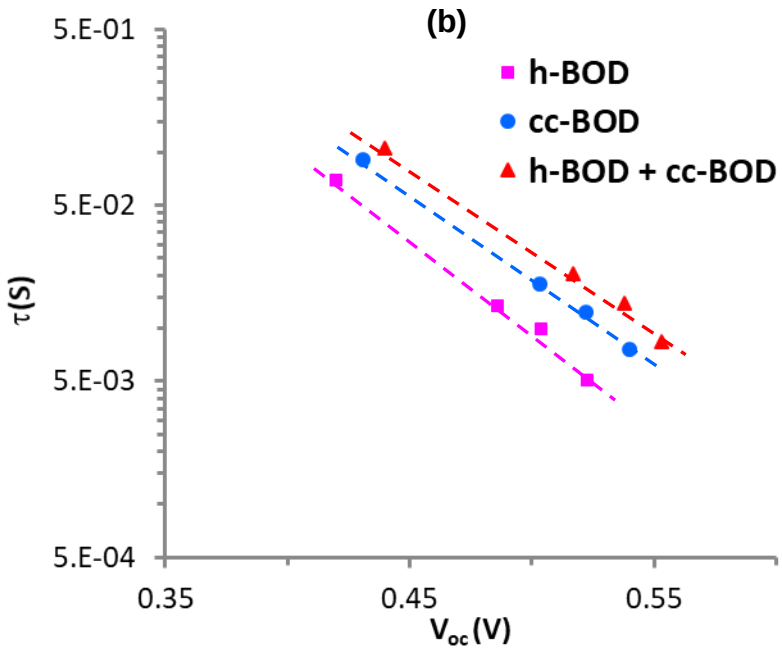

Figure 7. a) Electron density, and b) electron lifetime (τ) as a function of open-circuit photovoltage for DSSCs sensitized with ***h*-BOD**, ***cc*-BOD** single dye and ***h*-BOD** + ***cc*-BOD** dyes.

4. Conclusion

By combining the horizontal and vertical designs in one single dye, called *cross-conjugated design*, we designed and synthesized a new BODIPY-based dye, called cross-conjugated BODIPY, ***cc*-BOD**. It exhibits a strong a UV-visible-NIR absorption. Compared to a more standard BODIPY dye, using similar functional groups and based on a horizontal design, called ***h*-BOD**, the new ***cc*-BOD** exhibits clearly the highest conjugation and the highest light harvesting properties. Applied as photosensitizers in DSSCs, the ***cc*-BOD** dye has led to significantly higher photovoltaic performances than the ***h*-BOD,** with maximum PCE measured at 6.02 % instead of 3.7%. However, the simultaneous use of both dyes ***h*-BOD** + ***cc*-BOD as** co-sensitizer in DSSCs, led to a further PCE increase up to 6.2%, due to their complementary absorption properties. These results highlight the beneficial impact of our novel *cross-conjugated BODIPY-based design* in developing NIR dyes for the fabrication of high efficiency DSSCs.

Acknowledgements

This work was supported by the Deanship of Scientific Research (DSR), University of Jeddah, Jeddah, under grant No. (UJ-12-18-ICP). The authors, therefore, acknowledge with thanks DSR

technical and financial support. J.-J. L., T.H.C and A.I. acknowledges the support of NRF-2016M1A2A2940912 and 2015M1A2A2054996. A. I. also acknowledges the support from JSPS KAKENHI grant no. 18H02079.

Appendix A. Supporting information

Supplementary data associated with this article can be found in the online version at doi:000.

References:

1. B. O'regan and M. Grätzel, *nature*, 1991, **353**, 737.
2. M. Grätzel, *Journal of Photochemistry and Photobiology A: Chemistry*, 2004, **164**, 3-14.
3. M. Grätzel, *Inorganic chemistry*, 2005, **44**, 6841-6851.
4. A. Hagfeldt, G. Boschloo, L. Sun, L. Kloo and H. Pettersson, *Chemical reviews*, 2010, **110**, 6595-6663.
5. W. A. El-Said, M. Abdel-Shakour and A. M. Abd-Elnaiem, *Materials Letters*, 2018, **222**, 126-130.
6. Ö. Birel, S. Nadeem and H. Duman, *Journal of fluorescence*, 2017, **27**, 1075-1085.
7. J. Gong, K. Sumathy, Q. Qiao and Z. Zhou, *Renewable and Sustainable Energy Reviews*, 2017, **68**, 234-246.
8. Y. Chiba, A. Islam, Y. Watanabe, R. Komiya, N. Koide and L. Han, *Japanese journal of applied physics*, 2006, **45**, L638.
9. H. Tian, X. Yang, R. Chen, A. Hagfeldt and L. Sun, *Energy & Environmental Science*, 2009, **2**, 674-677.
10. L. Han, A. Islam, H. Chen, C. Malapaka, B. Chiranjeevi, S. Zhang, X. Yang and M. Yanagida, *Energy & Environmental Science*, 2012, **5**, 6057-6060.
11. G. Lingamallu, V. S. K. Jonnadula, K. Devulapally, T. H. Chowdhury, S. P. Singh, I. Bedja and A. Islam, *Journal of Materials Chemistry C*, 2019.
12. J.-H. Yum, E. Baranoff, S. Wenger, M. K. Nazeeruddin and M. Grätzel, *Energy & Environmental Science*, 2011, **4**, 842-857.
13. N. Duvva, G. Reddy, S. P. Singh, T. H. Chowdhury, I. Bedja, A. Islam and L. Giribabu, *New Journal of Chemistry*, 2019.

14. M. Abdel-Shakour, W. A. El-Said, I. M. Abdellah, R. Su and A. El-Shafei, *Journal of Materials Science: Materials in Electronics*, 2019, **30**, 5081-5091.
15. A. Mishra, M. K. Fischer and P. Bäuerle, *Angewandte Chemie International Edition*, 2009, **48**, 2474-2499.
16. Y. Ooyama and Y. Harima, *European Journal of Organic Chemistry*, 2009, **2009**, 2903-2934.
17. C. Qin, Y. Numata, S. Zhang, X. Yang, A. Islam, K. Zhang, H. Chen and L. Han, *Advanced Functional Materials*, 2014, **24**, 3059-3066.
18. M. M. Jadhav, T. H. Chowdhury, I. Bedja, D. Patil, A. Islam and N. Sekar, *Dyes and Pigments*, 2019, **165**, 391-399.
19. J. V. S. Krishna, N. V. Krishna, T. H. Chowdhury, S. Singh, I. Bedja, A. Islam and L. Giribabu, *Journal of Materials Chemistry C*, 2018, **6**, 11444-11456.
20. D. Patil, M. Jadhav, K. Avhad, T. H. Chowdhury, A. Islam, I. Bedja and N. Sekar, *New Journal of Chemistry*, 2018, **42**, 11555-11564.
21. K. Avhad, M. Jadhav, D. Patil, T. H. Chowdhury, A. Islam, I. Bedja and N. Sekar, *Organic Electronics*, 2019, **65**, 386-393.
22. Q. Huaulmé, A. Sutter, S. Fall, D. Jacquemin, P. Lévêque, P. Retailleau, G. Ulrich and N. Leclerc, *Journal of Materials Chemistry C*, 2018, **6**, 9925-9931.
23. A. Zampetti, A. Minotto, B. M. Squeo, V. G. Gregoriou, S. Allard, U. Scherf, C. L. Chochos and F. Cacialli, *Scientific reports*, 2017, **7**, 1611.
24. T. Kowada, H. Maeda and K. Kikuchi, *Chemical Society Reviews*, 2015, **44**, 4953-4972.
25. L. Huang, Z. Li, Y. Zhao, Y. Zhang, S. Wu, J. Zhao and G. Han, *Journal of the American Chemical Society*, 2016, **138**, 14586-14591.
26. I. Bulut, Q. Huaulmé, A. Mirloup, P. Chávez, S. Fall, A. Hébraud, S. Méry, B. Heinrich, T. Heiser and P. Lévêque, *ChemSusChem*, 2017, **10**, 1878-1882.
27. S. P. Singh and T. Gayathri, *European Journal of Organic Chemistry*, 2014, **2014**, 4689-4707.
28. H. Klfout, A. Stewart, M. Elkhalifa and H. He, *ACS applied materials & interfaces*, 2017, **9**, 39873-39889.
29. S. Kolemen, O. A. Bozdemir, Y. Cakmak, G. Barin, S. Erten-Ela, M. Marszalek, J.-H. Yum, S. M. Zakeeruddin, M. K. Nazeeruddin and M. Grätzel, *Chemical Science*, 2011, **2**,

949-954.

30. Y. Ooyama, Y. Hagiwara, T. Mizumo, Y. Harima and J. Ohshita, *New Journal of Chemistry*, 2013, **37**, 2479-2485.
31. J.-F. Lefebvre, X.-Z. Sun, J. A. Calladine, M. W. George and E. A. Gibson, *Chemical Communications*, 2014, **50**, 5258-5260.
32. D. Kumaresan, R. P. Thummel, T. Bura, G. Ulrich and R. Ziessel, *Chemistry–A European Journal*, 2009, **15**, 6335-6339.
33. Q. Huaulmé, C. Aumaitre, O. V. Kontkanen, D. Beljonne, A. Sutter, G. Ulrich, R. Demadrille and N. Leclerc, *Beilstein Journal of Organic Chemistry*, 2019, **15**, 1758-1768.
34. T. Bura, P. Retailleau and R. Ziessel, *Angewandte Chemie International Edition*, 2010, **49**, 6659-6663.
35. C. Qin, A. Mirloup, N. Leclerc, A. Islam, A. El- Shafei, L. Han and R. Ziessel, *Advanced Energy Materials*, 2014, **4**, 1400085.
36. A. Islam, T. H. Chowdhury, C. Qin, L. Han, J.-J. Lee, I. M. Bedja, M. Akhtaruzzaman, K. Sopian, A. Mirloup and N. Leclerc, *Sustainable Energy & Fuels*, 2018, **2**, 209-214.
37. G. Ulrich, C. Goze, M. Guardigli, A. Roda and R. Ziessel, *Angewandte Chemie International Edition*, 2005, **44**, 3694-3698.
38. A. Yella, H.-W. Lee, H. N. Tsao, C. Yi, A. K. Chandiran, M. K. Nazeeruddin, E. W.-G. Diau, C.-Y. Yeh, S. M. Zakeeruddin and M. Grätzel, *science*, 2011, **334**, 629-634.
39. T. Bura, N. Leclerc, S. Fall, P. Lévêque, T. Heiser, P. Retailleau, S. Rihn, A. Mirloup and R. Ziessel, *Journal of the American Chemical Society*, 2012, **134**, 17404-17407.
40. M. Mao, J.-B. Wang, Z.-F. Xiao, S.-Y. Dai and Q.-H. Song, *Dyes and Pigments*, 2012, **94**, 224-232.
41. A. Bessette and G. S. Hanan, *Chemical Society Reviews*, 2014, **43**, 3342-3405.
42. A. Hagfeldt and M. Graetzel, *Chemical Reviews*, 1995, **95**, 49-68.